The Cryosphere Discuss., 6, 4363–4385, 2012
www.the-cryosphere-discuss.net/6/4363/2012/
doi:10.5194/tcd-6-4363-2012

The Cryosphere Discussions

Variability of light transmission through Arctic land-fast sea ice during spring

M. Nicolaus[1], C. Petrich[2,3], S. R. Hudson[4], and M. A. Granskog[3]

[1]Alfred Wegener Institute for Polar and Marine Research, Bremerhaven, Germany
[2]Geophysical Institute, University of Alaska Fairbanks, Fairbanks, AK, USA,
[3]Northern Research Institute, Narvik, Norway
[4]Norwegian Polar Institute, Fram Centre, Tromsø, Norway

Received: 17 September 2012 – Accepted: 30 September 2012 – Published: 12 October 2012

Correspondence to: M. Nicolaus (marcel.nicolaus@awi.de)

Published by Copernicus Publications on behalf of the European Geosciences Union.

Abstract

The amount of solar radiation transmitted through Arctic sea ice is determined by the thickness and physical properties of snow and sea ice. Light transmittance is highly variable in space and time since thickness and physical properties of snow and sea ice are highly heterogeneous on variable time and length scales. We present field measurements of under-ice irradiance along repeated (March, May, June 2010) transects under un-deformed land-fast sea ice at Barrow, Alaska. The objective was to quantify seasonal evolution and spatial variability of light transmittance through snow and sea ice. Along with optical measurements, snow depth, sea ice thickness, and freeboard were recorded, and ice cores were analyzed for Chlorophyll *a* and particulate matter. Our results show that snow cover variability prior to onset of snow melt may cause as much spatial variability of relative light transmittance as the contrast of ponded and white ice during summer. In both instances, a spatial variability of up to three times above and below the mean was measured. In addition, we found a thirtyfold increase of light transmittance as a result of partial snowmelt. Hence, the seasonal evolution of transmittance through sea ice exceeded the spatial variability. Nevertheless, more comprehensive under-ice radiation measurements are needed for a more generalized and large-scale understanding of the under-ice energy budget for physical, biological, and geochemical applications.

1 Introduction

Physical properties and the thickness of sea ice and snow cover play a key role for the Arctic climate and ecosystems. They control the amount of solar irradiance reflected to the atmosphere, absorbed within snow and sea ice, and transmitted into the ocean beneath sea ice. Hence, they determine the surface radiation budget of the Arctic Ocean, and also impact global radiative forcing (Hudson, 2011).

TCD
6, 4363–4385, 2012

The interaction of sunlight and sea ice (incl. its snow cover) has been investigated in manifold studies at different places and during different seasons in the Arctic. In particular, the role of surface optical properties has been investigated extensively from in-situ observations (Grenfell and Perovich, 2004; Perovich et al., 1998, 2002b), numerical simulations (Grenfell, 1991; Gardner and Sharp, 2010; Light et al., 2003), laboratory experiments (Perovich and Grenfell, 1981), airborne measurements (Perovich et al., 2002a; Hanesiak et al., 2001), and remote sensing (Comiso and Kwok, 1996; Hall et al., 2004; Hall and Martinec, 1985; Tschudi et al., 2001). From these studies, wavelength-integrated (total or broadband) albedo is reasonably well quantified for different surface types, and the seasonal evolution is described in several ways for multi-year sea ice (Perovich et al., 2002a; Nicolaus et al., 2010a) and seasonal land-fast sea ice (Polashenski et al., 2012; Perovich et al., 1998; Perovich and Polashenski, 2012). Combining this seasonality with Arctic-wide datasets of sea-ice properties, Perovich et al. (2011) derived Arctic-wide estimates of energy fluxes into the sea ice (net solar short-wave irradiance). However, optical properties and in particular the surface albedo of first-year Arctic sea ice and melt ponds are still the subject of various studies, in particular with respect to its spatial and spectral variability. This is, because most studies of the last decades have concentrated on multi-year pack and land-fast sea ice.

Compared to surface albedo, little is known about the spatial and temporal variability of the amount of solar irradiance under sea ice (Ehn et al., 2011; Nicolaus et al., 2010a; Perovich et al., 1998; Gradinger et al., 2009; Light et al., 2008). One major challenge is accessibility of the under-ice environment, such that measurements are mostly limited to time-consuming spot measurements through bore holes. As a result, biologically and climatologically relevant energy budgets of specific regions and seasons cannot be given yet.

Connections between physical, biological, and optical properties of sea ice have long been recognized (Maykut and Grenfell, 1975; Grenfell and Maykut, 1977). The amount of sunlight transmitted though snow and sea ice into the upper ocean is of great importance for primary productivity and biogeochemical fluxes (Gradinger et al.,

TCD
6, 4363–4385, 2012

2009; Arrigo et al., 1991; Uusikivi et al., 2010), because it is the primary energy source. Under-ice measurements of solar irradiance have also been used to calculate biomass at the bottom of sea ice as a non-destructive method (Mundy et al., 2007).

A first comprehensive understanding of under-ice irradiance was achieved using data from SHEBA and radiative transfer simulations (Light et al., 2008). The first successful, long-term observations of transmitted irradiance through Arctic sea ice by an autonomous station, part of the drift of *Tara* in 2007, show a seasonality similar to that of surface albedo and highlight the importance of biological processes and their timing (Nicolaus et al., 2010a, b). The most detailed studies of spatial variability of light transmission through sea ice were performed under land-fast sea ice off Barrow, Alaska, by Perovich et al. (1998) and Maykut and Grenfell (1975). Maykut and Grenfell (1975) performed their measurements in early June 1972. They highlight the role of surface properties for light transmittance, and demonstrate the general shapes of spectra of transmitted irradiance for different surface conditions. Perovich et al. (1998) show total transmittances of 1 % during April, with variability of a factor four around the mean. This variability was mainly caused by differences in snow depth. Transmittance measurements through pond-covered sea ice, using divers showed how transmitted light spreads horizontally, affecting the light environment under ponded and white ice (Ehn et al., 2011). Along the same line, Petrich et al. (2012) showed through Monte Carlo simulations that light conditions at the bottom of sea ice are influenced by snow and sea-ice properties within a radius of 1 to 2 m. Unfortunately, comparisons across transmittance studies is hampered by the variability of snow, sea-ice, and weather conditions.

The goal of the presented study is to quantify the spatial and seasonal variability of solar short-wave transmittance through Arctic sea ice. To accomplish this, we performed in-situ measurements of solar irradiance along repeated horizontal transects under un-deformed land-fast sea ice off Barrow, Alaska, in March, May, and June of 2010. Our analyses quantify spatial and temporal variability of light transmission, focusing on the range of photosynthetically active radiation (PAR, 400 to 700 nm).

TCD
6, 4363–4385, 2012

2 Methods

Measurements were performed on level, seasonal, land-fast sea ice at the site of the sea-ice observatory at Barrow, Alaska (Druckenmiller et al., 2009), on 22 March, 14 May, and 11 June 2010. The site was chosen for the availability of supplementary data from seasonally installed radiation and ice mass balance stations. These stations provided a local record of incident, reflected, and transmitted spectral irradiance (Nicolaus et al., 2010b), ice thickness and temperature, snow depth, and atmospheric data (Druckenmiller et al., 2009). Water depth was approximately 6 m. All times given in this manuscript are in UTC, which is approximately 10.5 h ahead of local solar time.

Incident and transmitted solar irradiance were measured simultaneously with two upward-looking Ramses spectral radiometers with advanced cosine collectors (Ramses ACC, Trios GmbH, Rastede, Germany). Sensors, data processing, and data quality are discussed in detail by Nicolaus et al. (2010b). One sensor was mounted on a buoyant sled and operated under the sea ice (under-ice irradiance, Ew), and one sensor was mounted as surface reference (incident solar irradiance, Ed) approximately 1.5 m above the ice surface. Spectral and PAR transmittance, as well as mean values, were calculated as defined in Nicolaus et al. (2010b). The distance between the radiometer on the sled and the ice bottom was 2 ± 1 cm, varying slightly with under-ice topography. Spectra were not corrected for absorption between the sensor and the ice bottom. Pressure measurements from the under-ice radiometer were converted to depth in order to derive sea-ice draft for each spectrum.

The radiometer sled consisted of a buoyant frame, a means of propulsion, and an avalanche transmitter. Figure 1 shows the setup used in June measurements. The sled was deployed through a rectangular access hole cut through the ice (Fig. 2). Prior to the measurements, the sled was propelled forward with electric motors until resistance prevented further movement or the end of the tether line was reached, and then the motors were turned off. Radiation measurements were triggered for both sensors and the sled was manually pulled toward the access hole at increments of nominally

TCD
6, 4363–4385, 2012

0.5 m. After each 0.5 m pull, both sensors were again triggered. Measurements were performed around solar noon, and took approximately 1.5 h to complete.

The along-transect coordinate is the nominal path distance of the radiometer from the access hole. During transect measurements, the horizontal position of the radiometer was determined with an avalanche receiver (accuracy approx. 0.2 m) every 5 to 10 m. Corresponding radiometer measurements were tagged. These tie points were marked at the snow surface and later traced with a tape measure.

On 22 March, the access hole was located in the middle of the transect (Figs. 2a and 4a). From this hole, one 36 m and one 32 m long transect were measured in different directions under clear-sky conditions. Transect length was limited by under-ice topography that could not be passed since the sled had no means of vertical navigation. These two profiles were combined into one transect, consisting of 117 coincident measurements of incident and transmitted spectra. On 14 May, the access hole was at one end of an 80 m long transect (123 measurements, Figs. 2b and 4b) and the measurements were performed under overcast conditions with thin clouds. This transect length was limited by the cable length. On 11 June, two 20 m long transects were measured in similar directions from the access hole (Figs. 2c and 4c), because a strong current forced the sled in one particular direction. Transect lengths were again limited by under-ice topography. These two sub-profiles were combined into one transect, consisting of 71 paired spectral measurements. Cloud conditions were variable with changing fractions of clouds obstructing the solar disk. A compact camera was attached to the sled in June and programmed to take one photograph every 10 s. Flash was disabled and an indicator light on the camera was covered to prevent interference with optical measurements. The ice underside, the radiometer and parts of the sled were in the field of view; the camera was oriented toward the access hole (Fig. 1b).

After completing the radiation measurements, ice thickness and freeboard were measured though 5 cm-diameter auger holes spaced 5 m along each transect. Additional snow depth measurements were performed along the transect every 0.2 to 1.0 m. The transects were located within 100 m of the site of the observatory. Since

TCD
6, 4363–4385, 2012

data sets have different spatial resolutions, snow and ice data were interpolated to the locations of the spectral measurements. Observations that were obviously influenced by the respective access holes (2 to 5 m) were not included.

After each transect, a number of sea-ice cores were retrieved along the profiles for salinity, Chlorophyll *a* (Chl *a*), and particulate measurements (Table 1). In March, six cores were taken within few meters of the access hole. In May and June three and two cores were taken along the transects, respectively. All optical, thickness, and ice-core data are available online (Nicolaus et al., 2012).

3 Results and discussion

3.1 Thickness and melt of snow and sea ice

In March, the mean and standard deviation of sea-ice thickness was 1.28 ± 0.06 m, snow depth was 0.22 ± 0.08 m, and freeboard was mostly positive (Figs. 4 and 5). From the measurements in March to May, sea-ice thickness increased to 1.47 ± 0.06 m and snow depth increased to 0.27 ± 0.06 m, while modal snow depth remained unchanged at 0.25 m. Regular observations and measurements of surface albedo show that surface melt started after 5 June, with the first melt ponds forming after 9 June (Polashenski et al., 2012), causing a reduction in mean snow depth to 0.07 ± 0.03 m by the June measurements. Sea-ice thickness increased slightly to 1.50 ± 0.02 m. Freeboard was positive along the entire profile. The histograms in Fig. 5 illustrate that the range of sea-ice thickness and snow depth along the transects was largest in March and smallest in June. Changes in snow depth and snow properties can be seen in the photographs of surface conditions in Fig. 2, showing a visibly lower albedo and wet snow in June. These changes are expected to strongly influence the optical measurements under the sea ice, presented below.

TCD
6, 4363–4385, 2012

3.2 Sea-ice properties

Sea-ice salinity profiles measured during the March campaign showed C-shaped profiles typical of seasonal ice during the growth season, with the highest salinity of about 12 in the uppermost 0.05 m and a mean salinity of 7.2 (Table 1). In May, salinity profiles were very similar to the ones measured in March, containing just slightly more salt (mean 7.7). This indicates little if any flushing of sea ice until after our May transect. However, by 11 June the mean salinity decreased to 5.8, indicative of flushing. Physical inspection of the ice underside in June showed less pronounced lamellae depth than in March and May, with less biota visible than in May but more than in March. Vertically integrated Chl *a* concentrations of the sea ice increased from 0.5 mg m^{-2} in March to over 2.0 mg m^{-2} in May and 3.0 mg m^{-2} in June. Maximum concentrations as high as 35 mg m^{-3} were found in the bottommost 0.05 m in June. These concentrations are much lower than those found by Gradinger et al. (2009) at the same place during 2002. Also they are one to two orders of magnitude lower than those used by Mundy et al. (2007) for their parameterization of optical properties and biomass estimates, based on springtime observations in Resolute Passage, Canada. The amount of particulate matter in the ice cores remained constant at 11.0 mg m^{-2} in March, 11.3 mg m^{-2} in May, and 11.2 mg m^{-2} in June. The highest particulate concentrations were always found in the uppermost 0.2 m of sea-ice. Particulate concentrations in the snow were not measured.

3.3 Solar irradiance over and under sea ice

Incident irradiance of PAR, Ed_{PAR}, varied between the three campaigns. Due to differences in sky conditions, Ed_{PAR} was higher in May than in June. Also the degree of variability in Ed_{PAR} differed during the measurements; Ed_{PAR} varied only slightly (153 ± 8 W m^{-2}, 750 µE s^{-1} m^{-2}, ± denotes one standard deviation) in March under clear sky conditions, while Ed_{PAR} was more variable in May (262 ± 34 W m^{-2},

TCD
6, 4363–4385, 2012

1300 µE s^{-1} m^{-2}) and June (229 ± 31 W m^{-2}, 1150 µE s^{-1} m^{-2}), when the skies were overcast with changing cloud coverage (Table 1).

Transmitted solar irradiance recorded under sea ice, Et, varied significantly along each transect (spatial variability) and between the three transects (temporal evolution). Figure 4 shows the results of the under-ice measurements and illustrates the observed variability along each transect for three selected wavelengths in the PAR range (400, 550, and 700 nm) and for the total transmitted PAR Et_{PAR}. This variability was greatest in March, where profiles showed very different light conditions under sea ice. The first profile (negative x-values) had a range of Et_{PAR} up to 1.8 W m^{-2} (9 µE s^{-1} m^{-2}) while the second profile had very little variability with all fluxes below 0.5 W m^{-2} (2.5 µE s^{-1} m^{-2}). The largest fluxes were observed in June, when Et_{PAR} ranged up to 17.50 W m^{-2} (105 µE s^{-1} m^{-2}).

Comparing the three measurement dates, Et_{PAR} increased from 0.34 ± 0.17 W m^{-2} (1.8 µE s^{-1} m^{-2}) in March to 0.49 ± 0.36 W m^{-2} (2.5 µE s^{-1} m^{-2}) in May, and to 9.40 ± 4.31 W m^{-2} (50 µE s^{-1} m^{-2}) in June (Fig. 5). Most obvious here is the increase by a factor of 30 from before to after melt onset conditions. While these fluxes quantify light transmission through sea ice along the profiles and give an impression of the variability that might be expected, it is difficult to assess seasonal variability. Due to the large differences in Ed_{PAR} between the three campaigns and along each individual transect, it is difficult to directly compare the measurements of transmitted PAR, Et_{PAR}, with each other. Hence, we will concentrate on changes in transmittance in this manuscript, in order to assess the spatial variability and seasonal evolution in more detail.

3.4 Spectral and PAR Transmittance

Figure 3 shows transmittance spectra for each transect, one for lowest and one for highest transmittance on the transects, as well as the mean (average over all spectra along the transect) spectrum. Data quality was good, also for lowest light conditions.

TCD
6, 4363–4385, 2012

As expected all spectra show a smooth distribution of energy up to a wavelength of 750 nm. Beyond this, the ice is almost opaque. The wavelength of maximum transmittance increased slightly, from 523 nm in March, to 532 nm in May, and 536 nm in June, which would be consistent with an increase in colored dissolved organic matter (CDOM) (Granskog, 2012; Xu et al., 2012) although no indication for strong absorption peaks of Chl *a* can be found. For comparison, the seasonal study by Nicolaus et al. (2010a) in the transpolar drift showed only a little variability around 500 nm for the wavelength of maximum transmittance until the surface got water saturated. The shape of the transmittance spectra at Barrow changed only slightly, becoming wider, after melt onset. These changes were similar to those observed in the transpolar drift in 2007 (Nicolaus et al., 2010a) for the same time of the year. More pronounced change was observed later in the season, when a strong biological impact was observed on the transmitted spectra in the transpolar drift (Nicolaus et al., 2010a).

Mean transmittances of PAR, T_{PAR}, of 0.0019 and 0.0022 were very similar in March and in May (Fig. 5d), respectively, even the March value is strongly influenced by the section with thin snow, resulting in particularly high transmittance (Fig. 4a). This becomes obvious when comparing the ranges of T_{PAR} values: 0.0004 to 0.0113 in March and 0.0006 to 0.0035 in May. The minima are very similar, but the maximum was 3 times higher in March (Fig. 3). Accordingly, the snow-depth distribution between 0.2 and 0.3 m is similar in both months, but the May profile does not contain the thin snow depth observed in March. The mode of T_{PAR} (lowest bin, Fig. 5d) remained the same, combining the effects of a moderate decrease in modal snow thickness, from 0.28 to 0.24 m, and a slight increase in modal sea-ice thickness, by 0.19 m. Comparing T_{PAR} before and after melt onset (but before melt-pond formation), the values in March and May are over one order of magnitude lower than in June. From March to May, mean and modal T_{PAR} increased by 0.041 and 0.030, respectively. T_{PAR} was larger for every single measurement in June (ranging from 0.014 to 0.086) than for any measurement in March or May (Fig. 5d). Qualitatively, the same results hold for each wavelength of the spectra (Fig. 4). This increase occurred despite an increase of 0.22 m (17 %) in

TCD
6, 4363–4385, 2012

sea-ice thickness from March to June, as this small increase in ice thickness was more than offset by a 0.15 m (67 %) decrease in snow depth, illustrating the dominating role of snow in determining transmittance.

The relative range of transmittance around the mean (i.e. maximum/mean and mean/minimum) of T_{PAR} decreased over the season. This range was a factor of 6 to 7 in March (including the thin-snow area), about 3 in May, and only 2 to 3 in June. In other words, along each transect the transmittance ranged from about one third to three times the mean transmittance in May and June. Further into the melt season, when enhanced melting results in melt ponds and white ice, this range is expected to not increase, as implied by observations of Ehn et al. (2011) for first-year ice in the Canadian Arctic. They found transmittances of 0.05 to 0.16 for snow free white ice and 0.38 to 0.67 for melt ponds. This shows that pre-melt snow cover variations may cause as much spatial variability (in a relative sense) as the contrast of ponded and unponded summer sea ice. In addition, our observed variability in transmittance through spring snow and sea ice off Barrow, Alaska, matches well the results of Perovich et al. (1998) for the same region and season (April, before melt onset), which showed a variability between 0.0005 and 0.007 in transmittance along a 125 m long transect. These ranges represent the uncertainty that should be expected for a single spot measurement of under-ice radiation (e.g. Light et al., 2008; Gradinger et al., 2009) or stationary setups (Nicolaus et al., 2010a). For a detailed comparison of under-ice irradiance with snow depth the horizontal spreading of light in sea ice results has to be considered. This spread results in a 1 to 2 m footprint of the measurement, depending on ice-cover properties and solar zenith and azimuth angles (Ehn et al., 2011; Petrich et al., 2012). Hence, locally averaged snow depths should be considered in addition to ice thickness and ice type observations for the interpretation of optical measurements.

Comparing the spatial variability with the 30-fold seasonal increase of transmittances from March to June prior to melt-pond formation, it may be concluded that inter-seasonal variability is generally larger than spatial variability. Although this study contains only data from snow-covered sea ice, it is likely that this conclusion also holds

TCD
6, 4363–4385, 2012

for longer time series, reaching into summer conditions with melt ponds, when even more irradiance is transmitted (Ehn et al., 2011; Perovich, 1996). For comparison, transmittance of PAR was found to increase by a similar factor of 20 for multi-year ice in the transpolar drift during the drift of Tara (increase from 0.3 % at the end of April to 6 % in August, excluding biological effects, Nicolaus et al., 2010a). Also, the June measurements by Perovich et al. (1998) show a similar increase, although that study did not include transect measurements after melt onset. Another aspect is the vertical variability and distribution of solar irradiance under sea ice, and how this changes with seasons. This variability will depend on geometric features of ice conditions, as e.g. melt pond distributions (Frey et al., 2011), and on solar azimuth and zenith angles (Petrich et al., 2012), but also on the vertical distribution of biomass and other optically active substances.

This study confirms the importance of the role of snow for radiation transfer through snow and sea ice, as e.g. described by Warren (1982) and Perovich (1998). The effect of snow is a nearly wavelength-independent reduction of visible and near-UV transmittance, wavelengths at which absorption is low in pure ice and extinction is dominated by scattering, which is nearly wavelength independent (Warren et al., 2006). At longer wavelengths, where the absorption coefficient of ice increases, the significance of snow depth is reduced on thick ice since light will be absorbed by sea ice. With regard to the spectral composition of under-ice irradiance, biomass, CDOM, and sediments are most important (e.g. Gradinger et al., 2009; Perovich et al., 1993; Uusikivi et al., 2010).

3.5 Biomass estimates

In order to estimate sea-ice biomass from the optical measurements, the method of normalized difference indices (NDIs) was applied, as suggested by Mundy et al. (2007) based on data in Resolute Passage. Correlating these indices with snow depths, it was possible to show the independence of the method from snow depth and snow properties (data not shown). However, biomass estimates exceeded measurements by an order of magnitude (Table 1). It is assumed that the main reasons for this are that

TCD
6, 4363–4385, 2012

(1) Chl *a* concentrations in this study ($< 3\,\mu g\,m^{-2}$) were too low to allow the application of the algorithm from Resolute Passage (up to $110\,\mu g\,m^{-2}$), (2) the high load of particulate matter (up to $24\,mg\,m^{-2}$) in this study that affected spectral transmittance, (3) biological processes that change the pigment composition, e.g. regional differences in algal communities, and (4) non-linear aggregate effects at high abundances (possibly present in the data used by Mundy et al., 2007). It was also not possible to derive our own index based on the few ice-cores collected, or to use established methods from ocean-optics applications in the open ocean, since these include wavelengths around 670 nm which are strongly influenced by the snow cover (Perovich et al., 1993). Hence it is necessary to perform comprehensive sampling of ice cores and optical data, in order to derive improved methods to derive biomass estimates from under-ice irradiance measurements for a wider variety of ice types. And finally, this suggests it might be necessary to develop such methods individually for different ice types and locations, e.g. influenced by differences in particulate matter.

4 Conclusions

Repeated transects of under-ice radiation measurements on land-fast sea ice allowed to quantify seasonal and spatial variability of light conditions under sea ice. The measurements showed that the evolution of light transmittance from spring to summer (before and after melt onset) was much larger than the spatial variability along each transect. At the same time, relative spatial variability, i.e. the ratio between maximum/minimum and the mean transmittance, along each transect was similar before and after melt onset. However, all measurements were made before melt-pond formation. Variability in transmittance was dominated by the variability in snow depth and snow optical properties. In conjunction with increasing solar irradiance, the increase in transmittance results in the measured thirtyfold increase of light transmission over the seasons. Variability is of paramount importance for biological productivity and ice decay.

TCD
6, 4363–4385, 2012

Since the present measurements were taken directly at the ice-water interface of well-characterized land-fast sea ice the results provide a reference for measurements with remotely operated vehicles (ROVs) and autonomous underwater vehicles (AUVs). Conceivably, those studies enable extended transects close to the bottom of the ice in a variety of ice conditions found throughout the Arctic. It is suggested that these data sets include spectral data in order to distinguish processes, such as absorption by snow, sea-ice, biota, or sediments. While it would be sufficient to focus on the visible part of the spectrum, since snow and sea ice are almost opaque at longer and shorter wavelengths. Spectral water-column corrections may be necessary due to the extended distance from the ice. Data of the present study were obtained under snow-covered sea ice. Therefore, comprehensive large-scale data sets of snow depth and properties could be used to derive large-scale and more generalized estimates of under-ice irradiance. These estimates could be used to derive parameterizations to improve radiative transfer and energy budget parameterizations in numerical models. Future measurements should extend throughout the stages of melt-pond evolution and sea-ice decay, into freeze-up conditions, which may be more readily accomplished through ROV- and AUV-borne measurements. Also, efforts are needed to develop more generalized methods to use spectral radiation measurements under sea ice for biomass estimates. These methods may have to account for regional and seasonal differences, including the presence of particulate matter.

Acknowledgements. This project was based on the initiative and support of Sebastian Gerland (Norwegian Polar Institute, Tromsø) and Hajo Eicken (University of Alaska Fairbanks, UAF). We are most grateful for the exceptional support of field measurements by Dirk Kalmbach and Polona Itkin (both Alfred Wegener Institute, Bremerhaven, Germany, AWI), and Joshua Jones (UAF). Jennifer Peussner and Christian Katlein (both AWI) helped with the analysis of spectral data. Mette Kaufmann (UAF) kindly performed laboratory analyses of field samples. Data acquisition of the sea ice observatory at Barrow was funded under National Science Foundation grant no. OPP-0856867 (SIZONET). Manuscript preparation was supported by a German-Norwegian exchange program financed by the German-Norwegian bilateral research program

TCD
6, 4363–4385, 2012

of the Norwegian Research Council (NFR) (DAADppp program, grant 199844, and NFR grants 196143/S30, 197236/V30, and 195153).

References

Arrigo, K. R., Sullivan, C. W., and Kremer, J. K.: A bio-optical model of Antarctic sea ice, J. Geophys. Res., 96, 10581–10592, 1991.

Comiso, J. C. and Kwok, R.: Surface and radiative characteristics of the summer Arctic sea ice cover from multisensor satellite observations, J. Geophys. Res., 101, 28397–28416, doi:10.1029/96JC02816, 1996.

Druckenmiller, M. L., Eicken, H., Johnson, M. A., Pringle, D. J., and Williams, C. C.: Toward an integrated coastal sea-ice observatory: system components and a case study at Barrow, Alaska, Cold Reg. Sci. Technol., 56, 61–72, doi:10.1016/j.coldregions.2008.12.003, 2009.

Ehn, J. K., Mundy, C. J., Barber, D. G., Hop, H., Rossnagel, A., and Stewart, J.: Impact of horizontal spreading on light propagation in melt pond covered seasonal sea ice in the Canadian Arctic, J. Geophys. Res.-Oceans, 116, C00G02, doi:10.1029/2010jc006908, 2011.

Frey, K. E., Perovich, D. K., and Light, B.: The spatial distribution of solar radiation under a melting Arctic sea ice cover, Geophys. Res. Lett., 38, L22501, doi:10.1029/2011gl049421, 2011.

Gardner, A. S. and Sharp, M.: A review of snow and ice albedo and the development of a new physically based broadband albedo parameterization, J. Geophys. Res., 115, F01009, doi:10.1029/2009JF001444, 2010.

Gradinger, R. R., Kaufman, M. R., and Bluhm, B. A.: Pivotal role of sea ice sediments in the seasonal development of near-shore Arctic fast ice biota, Mar. Ecol.-Prog. Ser., 39449–39463, doi:10.3354/meps08320, 2009.

Granskog, M.: Changes in spectral slopes of colored dissolved organic matter absorption with mixing and removal in a terrestrially dominated marine system (Hudson Bay, Canada), Mar. Chem., 134–135, 10–17, doi:10.1016/j.marchem.2012.02.008, 2012.

Grenfell, T. C.: A radiative transfer model for sea ice with vertical structure variations, J. Geophys. Res., 96, 16991–17001, 1991.

Grenfell, T. C. and Maykut, G. A.: The optical properties of ice and snow in the Arctic basin, J. Glaciol., 18, 18445–18463, 1977.

TCD
6, 4363–4385, 2012

Grenfell, T. C., and Perovich, D. K.: Seasonal and spatial evolution of albedo in a snow-ice-land-ocean environment, J. Geophys. Res., 109, C01001 doi:10.1029/2003JC001866, 2004.
Hall, D. K. and Martinec, J.: Remote Sensing of Ice and Snow, Chapman and Hall, London, 189 pp., 1985.
Hall, D. K., Key, J. R., Casey, K. A., Riggs, G. A., and Cavalieri, D. J.: Sea ice surface temperature product from MODIS, IEEE T. Geosci. Remote, 42, 1076–1087, 2004.
Hanesiak, J. M., Barber, D. G., De Abreu, R. A., and Yackel, J. J.: Local and regional albedo observations of Arctic first-year sea ice during melt ponding, J. Geophys. Res., 106, 1005–1016, 2001.
Hudson, S. R.: Estimating the global radiative impact of the sea ice-albedo feedback in the Arctic, J. Geophys. Res.-Atmos., 116, D16102, doi:10.1029/2011jd015804, 2011.
Light, B., Maykut, G. A., and Grenfell, T. C.: A two-dimensional Monte Carlo model of radiative transfer in sea ice, J. Geophys. Res.-Oceans, 108, 3219, doi:10.1029/2002jc001513, 2003.
Light, B., Grenfell, T. C., and Perovich, D. K.: Transmission and absorption of solar radiation by Arctic sea ice during the melt season, J. Geophys. Res., 113, C03023, doi:10.1029/2006JC003977, 2008.
Maykut, G. A. and Grenfell, T. C.: Spectral distribution of light beneath 1st-year sea ice in Arctic Ocean, Limnol. Oceanogr., 20, 554–563, 1975.
Mundy, C. J., Ehn, J. K., Barber, D. G., and Michel, C.: Influence of snow cover and algae on the spectral dependence of transmitted irradiance through Arctic landfast first-year sea ice, J. Geophys. Res., 112, C03007, doi:10.1029/2006JC003683, 2007.
Nicolaus, M., Gerland, S., Hudson, S. R., Hanson, S., Haapala, J., and Perovich, D. K.: Seasonality of spectral albedo and transmissivity as observed in the Arctic Transpolar Drift in 2007, J. Geophys. Res., 115, C11011, doi:10.1029/2009JC006074, 2010a.
Nicolaus, M., Hudson, S. R., Gerland, S., and Munderloh, K.: A modern concept for autonomous and continuous measurements of spectral albedo and transmittance of sea ice, Cold Reg. Sci. Technol., 62, 14–28, 2010b.
Perovich, D. K.: The Optical Properties of Sea Ice, Cold Regions Research and Engeneering Laboratory Monograph, 96-1, 1996.
Perovich, D. K. and Grenfell, T. C.: Laboratory studies of the optical properties of young sea ice, J. Glaciol., 27, 331–346, 1981.
Perovich, D. K. and Polashenski, C.: Albedo evolution of seasonal Arctic sea ice, Geophys. Res. Lett., 39, L08501, doi:10.1029/2012GL051432, 2012.

TCD
6, 4363–4385, 2012

Perovich, D. K., Cota, G. F., Maykut, G. A., and Grenfell, T. C.: Bio-optical observations of first-year Arctic sea ice, Geophys. Res. Lett., 20, 1059–1062, 1993.
Perovich, D. K., Roesler, C. S., and Pegau, W. S.: Variability in Arctic sea ice optical properties, J. Geophys. Res.-Oceans, 103, 1193–1208, 1998.
Perovich, D. K., Grenfell, T. C., Light, B., and Hobbs, P. V.: Seasonal evolution of the albedo of multiyear Arctic sea ice, J. Geophys. Res., 107, 8044, doi:10.1029/2000JC000438, 2002a.
Perovich, D. K., Tucker, W. B., and Ligett, K. A.: Aerial observations of the evolution of ice surface conditions during summer, J. Geophys. Res., 107, 8048, doi:10.1029/2000JC000449, 2002b.
Perovich, D. K., Jones, K. F., Light, B., Eicken, H., Markus, T., Stroeve, J., and Lindsay, R.: Solar partitioning in a changing Arctic sea-ice cover, Ann. Glaciol., 52, 192–196, 2011.
Petrich, C., Nicolaus, M., and Gradinger, R.: Sensitivity of the light field under sea ice to spatially inhomogeneous optical properties and incident light assessed with three-dimensional Monte Carlo radiative transfer simulations, Cold Reg. Sci. Technol., 73, 1-11, doi:10.1016/j.coldregions.2011.12.004, 2012.
Polashenski, C., Perovich, D., and Courville, Z.: The mechanisms of sea ice melt pond formation and evolution, J. Geophys. Res.-Oceans, 117, C01001, doi:10.1029/2011jc007231, 2012.
Tschudi, M. A., Curry, J. A., and Maslanik, J. A.: Airborne observations of summertime surface features and their effect on surface albedo during FIRE/SHEBA, J. Geophys. Res., 106, 15335–15344, 2001.
Uusikivi, J., Vähätalo, A. V., Granskog, M. A., and Sommaruga, R.: Contribution of mycosporine-like amino acids and colored dissolved and particulate matter to sea ice optical properties and ultraviolet attenuation, Limnol. Oceanogr., 55, 703–713, 2010.
Warren, S. G.: Optical properties of snow, Rev. Geophys. Space Ge., 20, 67–89, 1982.
Warren, S. G., Brandt, R. E., and Grenfell, T. C.: Visible and near-ultraviolet absorption spectrum of ice from transmission of solar radiation into snow, Appl. Optics, 45, 5320–5334, doi:10.1364/ao.45.005320, 2006.
Xu, Z., Yang, Y., Wang, G., Cao, W., Li, Z., and Sun, Z.: Optical properties of sea ice in Liaodong Bay, J. Geophys. Res., 117, C03007, doi:10.1029/2010JC006756, 2012.

TCD
6, 4363–4385, 2012

Table 1. Vertically integrated sea-ice properties from all full-length cores obtained during the measurements in 2010. Missing values were not measured. Full profile data are available online from Nicolaus et al. (2012).

Date	Core	Core length (m)	Salinity	Chlorophyll *a* ($\mu g\,m^{-2}$)	Particulate matter ($mg\,m^{-2}$)
19 Mar	A	1.29	7.7	0.85	
	B	1.29	6.6		12.55
20 Mar	A	1.32	7.6	0.33	
	B	1.30	7.7		9.76
	C	1.26	7.3		10.59
	D	1.25	6.3	0.39	
13 May	C	1.53	8.3	2.29	23.94
14 May	A	1.41	7.2	0.54	5.52
	B	1.53	7.5	3.00	4.46
11 Jun	A	1.55	5.6	2.11	6.52
	B	1.45	6.0	3.82	15.87

TCD
6, 4363–4385, 2012

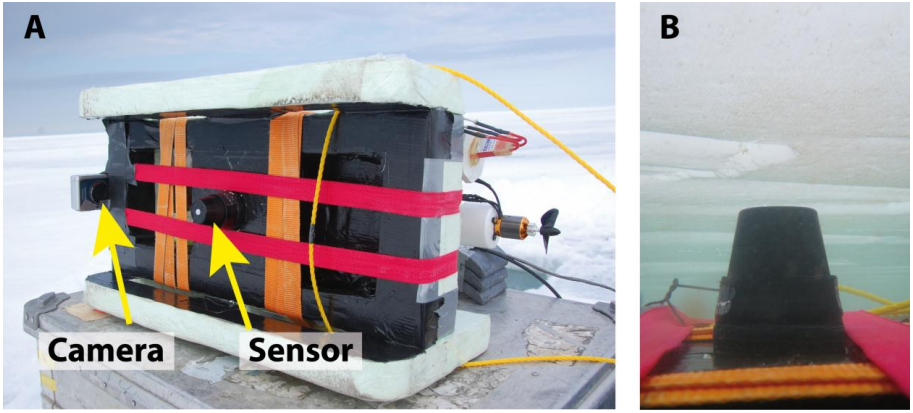

Fig. 1. (A) Sled lying on its side with radiometer in the center, a backward-looking on-board camera, and the yellow tether line at the back of the sled. The straps tie the propulsion to the sled (motor, speed controller and weights). **(B)** Photograph taken by the on-board camera during under-ice operations in June. The underside of the ice close to the sensor is white while ice in the distance appears to be cyan presumably because of preferential absorption of red light in water.

TCD
6, 4363–4385, 2012

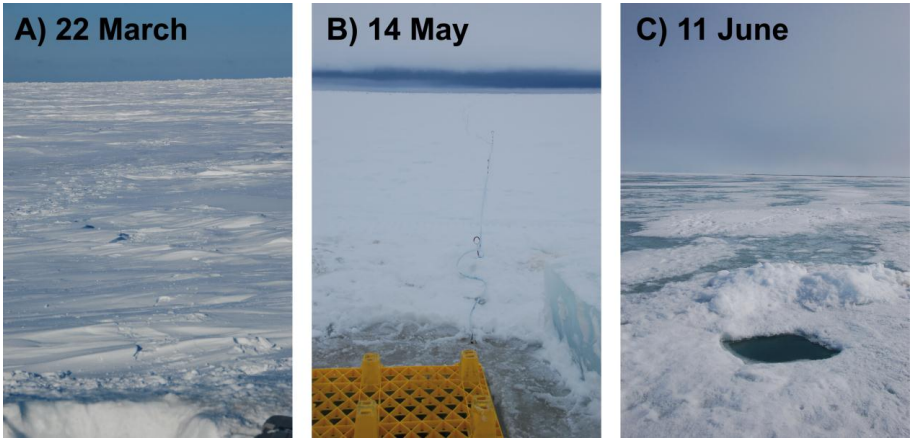

Fig. 2. Photographs of surface conditions along profiles in **(A)** March, **(B)** May, and **(C)** June 2010. All photographs were taken after completion of the measurements, which were performed under un-disturbed surfaces. The snow pile next to the hole in June resulted from the hole construction. This part was removed for analyses.

TCD
6, 4363–4385, 2012

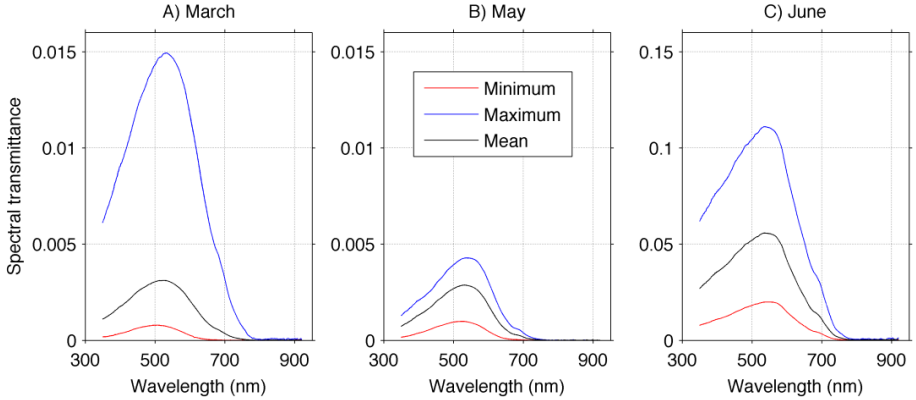

Fig. 3. Spectral transmittance through snow and sea ice in **(A)** March, **(B)** May, and **(C)** June 2010. For each transect the spectra for minimum and maximum light conditions as well as the mean spectrum for the transect are given. Note different scales (factor 10) for the data in June.

TCD
6, 4363–4385, 2012

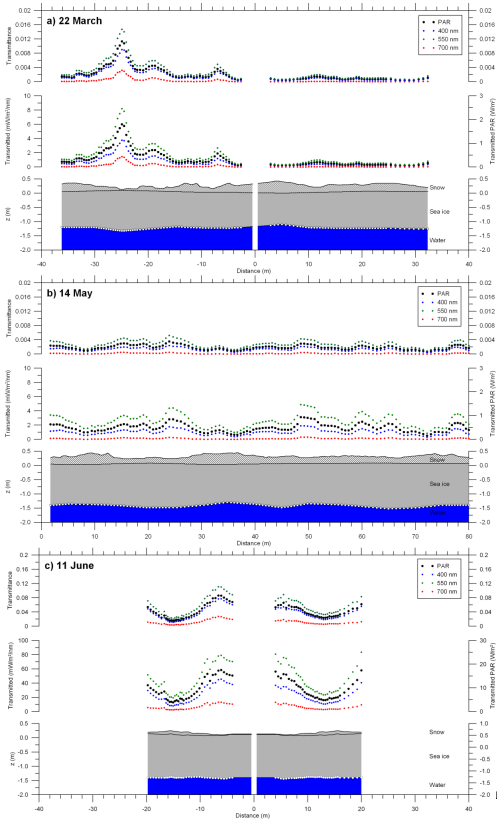

Fig. 4. Transect geometry (bottom), transmitted irradiance (middle), and transmittance (top) of snow and sea ice for each of the three transects in **(a)** March, **(b)** May, and **(c)** June 2010. Radiation data are given for photosynthetically active radiation (PAR, black circles) and spectral values at 400 nm (blue dots), 550 nm (green dots), and 700 nm (red dots). Note different scales (factor 10) on radiation data in June. $x = 0$ denotes the center of the access hole of the sled.

TCD
6, 4363–4385, 2012

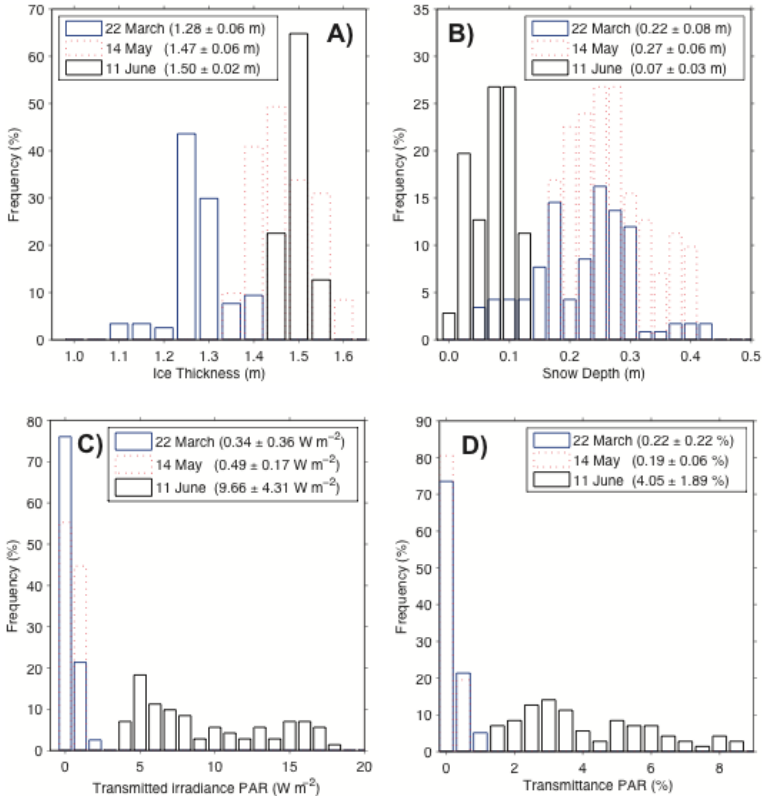

Fig. 5. Frequency distributions of **(A)** Sea-ice thickness and **(B)** snow depth **(C)** transmitted irradiance of PAR, and **(D)** Transmittance of PAR along the transects. Mean values of all distributions are given as mean ± one standard deviation in the legends.

TCD
6, 4363–4385, 2012

Variability of light transmission through Arctic land-fast sea ice

M. Nicolaus et al.